Hindawi
Mathematical Problems in Engineering
Volume 2019, Article ID 8156450, 14 pages
https://doi.org/10.1155/2019/8156450

Research Article

A Study of Probabilistic Diagnosis Method for Three Kinds of Internal Combustion Engine Faults Based on the Graphical Model

Jiameng Liu, Bo Ma, and Zhinong Jiang

Beijing Key Laboratory of High-End Mechanical Equipment Health Monitoring and Self-Recovery, Beijing University of Chemical Technology, Beijing, China

Correspondence should be addressed to Zhinong Jiang; 2014400121@mail.buct.edu.cn

Received 10 December 2018; Revised 2 March 2019; Accepted 31 March 2019; Published 11 April 2019

Academic Editor: Zhi-ke Peng

A strategy for increasing the accuracy rate of internal combustion engine (ICE) fault diagnosis based on the probabilistic graphical model is proposed. In this method, a three-layer network with inference of probability is constructed, and both the material conditions and the signals collected from different engine parts are considered as the inputs of the system. Machine signals measured by sensors were processed in order to diagnose potential faults, which were presented as probabilities based on the components in layer 1, fault categories in layer 2, and fault symptoms in layer 3. The diagnosis model was built by using nodes and arcs, and the results depended on the connections between the fault categories and symptoms. The parameters of the network represented quantitative probabilistic relationships among all layers, and the conditional probabilities of each type of fault and relevant symptoms were summarized. Fault cases were simulated on a 12-cylinder diesel engine, and three fault types that often occur on ICEs were tested based on five different fault symptoms with different loads, respectively. The diagnostic capability of the method was investigated, reporting high accuracy rates.

1. Introduction

Internal combustion engines (ICEs) play a significant role in the energy supply of basic industrial applications, often working for long periods without stopping. Any fault in the ICE would interrupt the production process, bring significant economic losses, and even harm the operators on the spot if severe damage happens with explosion. Therefore, it is important to monitor the engine status during the running process for the fault diagnosis.

ICE fault diagnosis has been studied since the invention of ICEs, and over the past several decades, different methods have been proposed by researchers. Wavelet packet [1–5] has been developed and applied in the field of ICE fault diagnosis. A fault diagnosis system using wavelet packet transform and artificial neural network techniques has been proposed by Wu and Liu [6]. The application of wavelet transform in machine condition monitoring and fault diagnostics has been summarized by Peng and Chu [7]. Fault feature extraction using algorithm of sparse analysis [8, 9] and size estimation method [10] has been studied. A novel fault localization method has been proposed by Cui et al. [11]. Convolutional neural network [12] and Bayesian diagnosis method [13, 14] have been proposed. Several other methods, the Monte Carlo method [15], the fuzzy diagnosis method [16], and the support vector machine (SVM) method [17, 18], have been also applied in machine fault diagnosis with good performance. Additionally, novel approaches like Switching Unscented Kalman Filter method [19], Extreme Learning Machines [20], Online Dictionary Learning [21], and the discriminative nonnegative matrix factorization (DNMF) method [22] have been proposed. As a branch of applied artificial intelligence (AI), expert systems are also introduced in the field of fault diagnosis and have been built demonstrating good performances [23–25].

Although some promising results have been achieved by previous studies, there is still a need for improvement in a number of aspects. Firstly, taking into consideration

only a single type of signal as the diagnostic input cannot accurately reflect the running state of the engine. Due to the fact that one type of fault may lead to several symptoms, various state signals need to be collected from the machine and be used in the diagnostic process of the system. Secondly, only one kind of fault category has been reported for each method. An advanced system should be able to cope with common faults that may occur during the running process, and multiple faults can be diagnosed at the same time. Thirdly, there is no evidence that a specific engine symptom can be exclusively used as the unique signal of a fault, and thus a probability model should be introduced in the process able to describe the equipment state in a more precise manner than just indicating the existence or not of the fault. The probability of a signal that represents a sign of potential fault should be considered.

The inference results should be associated with a probability that can describe the state of the engine precisely. The probabilistic graphical model is a combination of the graph theory with the probability theory, which is suitable for dealing with complex systems [26]. In the present study, in order to overcome the aforementioned problems, a method for three kinds of ICE faults using a probabilistic graphical model is presented. The inference engine of the system was established based on the probabilistic graphical model. Combined information on the machine vibration and rotation speeds was simultaneously collected and used as the system input. Various fault symptoms that occurred together during the running of the engine were taken into consideration. Three fault categories were set as the outputs of the system during the experiments, and eight cases for each category were studied. The results demonstrated a high accuracy rate.

2. The Probabilistic Graphical Model

2.1. The Bayesian Theory. The probabilistic graphical model, consisting of a directed acyclic graph (DAG) with nodes and arcs, can model the causal relationships between several facts represented by nodes connected to each other with directed arcs since the occurrence probability of a node can be calculated by the independent probability and the conditional probability. The Noisy-OR gate was introduced in order to improve the diagnosis accuracy and enhance the robustness of the system. The leak Noisy-OR gate, a calculation module, can solve a problem with a large number of parameters by modeling the conditional probability, which, due to the complex working environment, is often extremely time consuming in the construction of the system.

Considering that event A and event B are independent to each other, the conditional probability of event A given event B is denoted as P(A | B) and is defined as

$$\mathrm{P}(\mathrm{AB}) = \frac{P(AB)}{P(B)} = \frac{P(A)\,P(B \mid A)}{P(B)} \tag{1}$$

where P(AB) is the joint probability.

Assume that $\mathrm{P}(B_i) > 0,\ i = 1, 2, \ldots, n, \sum_{i=1}^{n} B_i = S$, where S is a certain event, and B_i hypotheses are mutually exclusive.

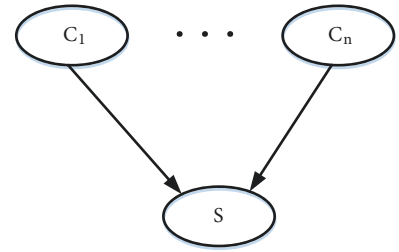

Figure 1: Simple probabilistic graphical model.

When the events $B_1, B_2, \ldots, B_n$ are a set of random variables, the probability of A is

$$\mathrm{P}(\mathrm{A}) = \sum_{i=1}^{n} P(B_i)\,P(A \mid B_i) \tag{2}$$

and the posterior probability of B_i is

$$\mathrm{P}(B_i \mid \mathrm{A}) = \frac{P(AB_i)}{P(A)} = \frac{P(B_i)\,P(A \mid B_i)}{\sum_{n}^{i=1} P(B_i)\,P(A \mid B_i)} \tag{3}$$

A classic probabilistic graphical model can be seen in Figure 1, and there are three necessary requirements for the construction of the Noisy-OR gate model:

(1) All nodes in the network must be binary, which means that every node can have only two states, True (T) or False (F).

(2) For each node S and its parent nodes $C_n, C_1, C_2, \ldots, C_n$ must be independent of each other.

(3) For each parent node there is a probability of connection: $P_i = (\mathrm{S} \mid \mathrm{C}_i) = \mathrm{P}(\mathrm{S} \mid \overline{C_1}, \overline{C_2}, \ldots, \mathrm{C}_i, \ldots, \overline{C_n})\ i \in n$, which is the probability of node S whose state is T when C_i is T and other states of its parent nodes are F.

The probability that event S is in true state is

$$\mathrm{P}(\mathrm{S} = T \mid H) = 1 - \prod_{i:C_i \in H^+} (1 - P_i) \tag{4}$$

where H is the entire parent set of nodes of S, and H^+ is the subset of H nodes that are in true state. However, if H^+ is the empty set, the value of $\mathrm{P}(\mathrm{S} = T \mid H)$ would be zero. Due to the fact that there would be no zero probability in the industrial processes, the leak Noisy-OR gate was applied for the solution.

2.2. The Leak Noisy-OR Gate. It is possible that a fault of the machine can be a result of symptoms not included in the cause nodes, and the diagnosis system cannot be built explicitly with all possible causes. Thus, the leak probability should be included in the model [27–29].

The leak Noisy-OR gate is introduced in the probabilistic graphical model as shown in Figure 2. All the events that are unclear are collected in one node, denoted by C_L, with the probability P_L.

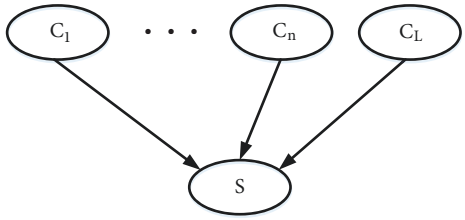

Figure 2: The probabilistic graphical model with the leak Noisy-OR gate.

The leak probability can be calculated as

$$P_l = \sum_{i=1}^{n} \left[1 - P\left(C_i\right)\right] P_l^i \tag{5}$$

After the probabilities of $P_1, P_2, \ldots, P_n$ are calculated, the conditional probability table (CPT) can be obtained based on

$$\mathrm{P}\left(\mathrm{S} = T \mid H\right) = 1 - \left(1 - P_l\right) \prod_{i:C_i \in H^+} \left(1 - P_i\right) \tag{6}$$

2.3. The Prior Probability of the Model. The prior probabilities of the whole model depend on the survival probability of the materials and can be affected by the current material properties of the engine components during running conditions. The movement of the pistons and the conrods with the crankshaft can be defined by the reciprocating linear motion of the piston and the rotary motion of the crankshaft. The inertial force can be described as the combination of the reciprocating inertial force generated by the reciprocating mass with the centrifugal force generated by the rotating mass. As such, the prior probabilities can be described by the Probabilistic-S-N curve (P-S-N curve) of the material [30] based on the Bayesian theory. According to the probability model presented by Feng et al. [31], the survival probability density function of a material parameter is

$$\mathrm{P} = \mathrm{Fr}\left(\mathrm{T} = \ln N\right) \tag{7}$$

where N is the fatigue life of the component and T is the number of cycles. The prior probabilities can be obtained from that combined with data handbook [32].

3. The Fault Diagnosis System

3.1. The Three-Layer Structure. The logic system is made up of nodes and arcs. The nodes are divided into three different layers: the upper layer, the middle layer, and the lower layer [33]. The arcs are the links between nodes in neighboring layers, but there are no direct links from the upper to the lower layer. Therefore, all the arcs from upper layer nodes point to middle layer nodes, and the arcs from middle layer nodes point to lower layer nodes.

The first layer, which is called the component layer, consists of key components of the engine related to the probabilities of fault occurrence that can affect the fault prior probabilities. In this layer, the states of the nodes provide the network with prior probability in the calculation process. Any adjustments in the states of the first layer nodes will influence the fault nodes in the second layer. The second layer, which is called the fault layer, consists of different types of fault that may occur in the engine. Each type of fault is represented by one node. After the calculation, each node will be in a determined state, with a percentage indicating the probability of the correspondent fault to occur during the running. The third layer, which is called fault symptom layer, consists of several engine characteristics. The working state information of the engine can be measured and transmitted to a computer, where the engine signals, which can reflect fault symptoms, will activate the related nodes in this layer. Then, the activated nodes will turn to the fault state, which is also T state meaning there exists a kind of fault, and the calculation will proceed to the second layer. The three-layer structure is shown in Figure 3.

For the CPT construction, assuming that $\mathrm{P}(\mathrm{S} \mid \overline{C_i}) = P_{all}$, $\mathrm{P}(S \mid C_i)$ can be obtained according to (4),

$$\mathrm{P}\left(S \mid C_i\right) = P_i + P_{all} - P_i P_{all} \tag{8}$$

and the connection probability P_i of the parent nodes of S can be calculated based on (8):

$$P_i = \frac{\mathrm{P}\left(\mathrm{S} \mid C_i\right) - \mathrm{P}\left(\mathrm{S} \mid \overline{C}_i\right)}{1 - \mathrm{P}\left(\mathrm{S} \mid \overline{C}_i\right)} \tag{9}$$

since P_l^i can be obtained by the following equation to get P_l.

$$\begin{aligned} \mathrm{P}\left(\overline{S} \mid C_i = F\right) &= \frac{\sum_{\mathrm{H}|C_i \in H^-} P\left(\overline{S} \mid \mathrm{H}\right) P\left(H\right)}{P\left(C_i = F\right)} \\ &= \frac{\sum_{\mathrm{H}|C_i \in H^-} \left(1 - P_l^i\right) \prod_{C_j \in H^+} \left(1 - P_j\right) \prod\limits_{C_j \in H^+} P\left(C_j\right) \prod_{C_j \in H^-} P\left(\overline{C}_j\right)}{P\left(\overline{C_i}\right)} \end{aligned} \tag{10}$$

For the prior probabilities based on (7),

$$\mathrm{P} = \int_{-\infty}^{\ln N} \frac{1}{\sigma\sqrt{2\pi}} \exp\left(-\frac{\left(\ln N - \mu\right)^2}{2\sigma^2}\right) d \ln N \tag{11}$$

Here $\mathrm{N} = e^T$ obeys the lognormal distribution. Since we have standard normal distribution variable which is denoted by

$$\mathrm{z} = \frac{\ln N - \mu}{\sigma} \tag{12}$$

the distribution function of standard normal distribution is

$$\Phi\left(\mathrm{z}\right) = \int_{-\infty}^{z} \frac{1}{\sqrt{2\pi}} e^{-z^2/2} dz \tag{13}$$

Then the prior probabilities of engine component of fault in the ICE can be

$$\mathrm{P} = 1 - \Phi\left(\mathrm{z}\right) = \frac{1}{\sqrt{2\pi}} \int_{z}^{-\infty} e^{-z^2/2} dz \tag{14}$$

Table 1: The node IDs of the third layer.

Node	Node ID
High vibration speed value	H_VibS_PV
High vibration acceleration value	H_VibA_PV
Low transient rotation speed value	L_Tran_S
Low kurtosis value	L_Kurt
High torsional vibration value	H_TorP_PPV

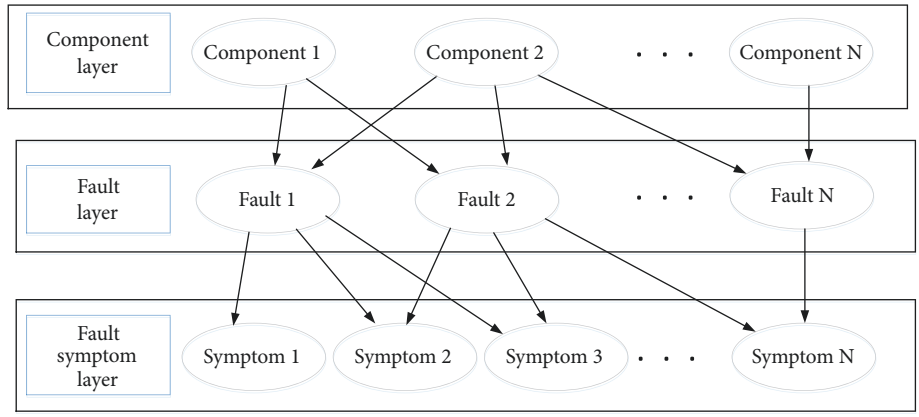

Figure 3: The three-layer logic structure.

3.2. The Establishment of the Model. For the ICE fault diagnosis, the engine performance information can be detected by sensors and transmitted to the computer that runs the system. The probability of the potential fault can be calculated by the inference engine.

Sensors are placed on key parts of the ICE in order to collect useful information. Vibration piezoelectric and eddy current sensors are placed on the surface of the engine in order to collect running state information, which will be transferred to the data collector. Before the inference procedure, all signals are processed using a denoising filter. Then the information collected in the computer storage will be processed and analyzed. The combination of the acquired data can reveal the current state of the machine.

The system was established based on diagnostic rules acquired from experts, published papers [34–36], or experimental knowledge. Each signal collected by the sensors and transmitted to the computer is compared to a threshold value that determines the node state, which is set beforehand by an expert at the initialization of the system. Based on a single signal or a combination of signals, different fault probabilities can be calculated, depending on if the value is above or below the threshold. The third-layer nodes and the corresponded IDs can be seen in Table 1, while the corresponding relations between the signals and the fault types among the three layers is illustrated in Figure 4. When the input signal is transmitted into the system, the component layer and the symptom layer nodes will affect the fault layer. The direct interactions between any two nodes of adjacent layers are presented.

The upper layer contains information about the current condition of the key ICE components, which is related to the fault types in the second layer. The key engine components are the cylinder, the piston, and the bearing. As it can be seen in Figure 4, each node in first layer is connected to one or more nodes in the middle layer.

The second layer is the fault layer and contains nodes of three different fault categories that may occur: cylinder knock fault, cylinder score fault, and bearing wear fault. The fault nodes are independent of each other but they can be activated at the same time. There is a node of leak fault in this layer containing the leak probability with Noisy-OR gate. The leak node of fault is connected to every node in the third layer with directed arcs.

The third layer contains the fault characteristics that can be detected, according to the parameter thresholds, directly from the signals. Once the value of the current signal is above or below the threshold value, the state of the node is activated. The system will analyze the signals to deduce the fault possibility based on the knowledge base.

The prior probabilities of the different components are set independently according to the parameters of each component, and the leak probabilities are set to 0.001 as default. Based on previously collected fault case data and experience, a probability analysis is performed by the system, setting the conditional probabilities of the initial parameters, which can be adjusted with experiences (Table 2).

4. Experiments on a Diesel Engine

4.1. Test Procedure and Results. A 12-cylinder diesel engine (Figure 5) was used as the fault simulation testbed for the case study. Several different fault-related signals were measured by the sensors, while the machine was operated under a

Table 2: Conditional probability table of the symptoms.

Symptom ID	Cylinder knock	Bearing wear	Cylinder score
H_VibS_PV	0.88	0.85	0
H_VibA_PV	0.76	0	0.89
L_Tran_S	0	0.67	0
H_Kurt	0	0.85	0
H_TorP_PPV	0	0	0.79

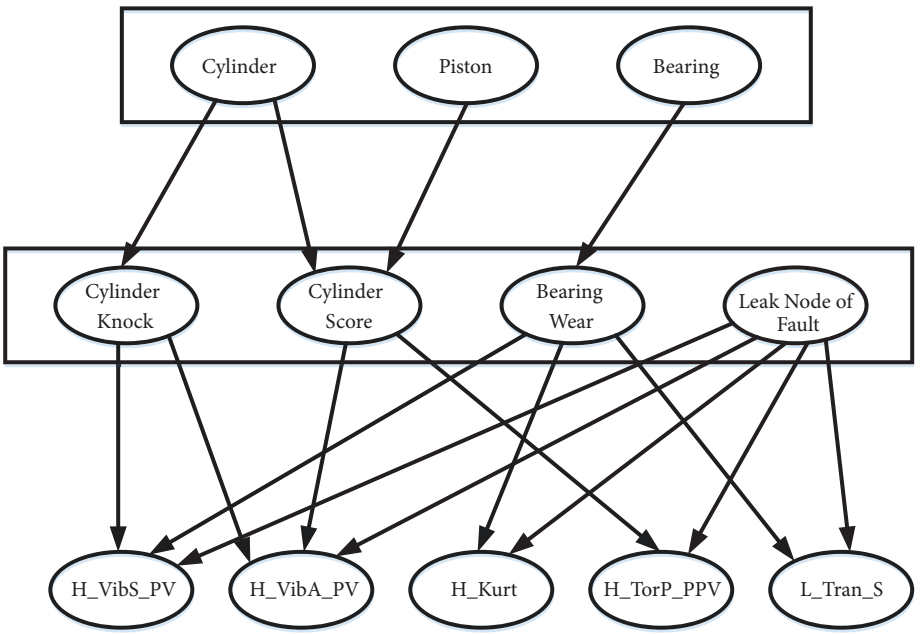

Figure 4: Three-layer structure with nodes.

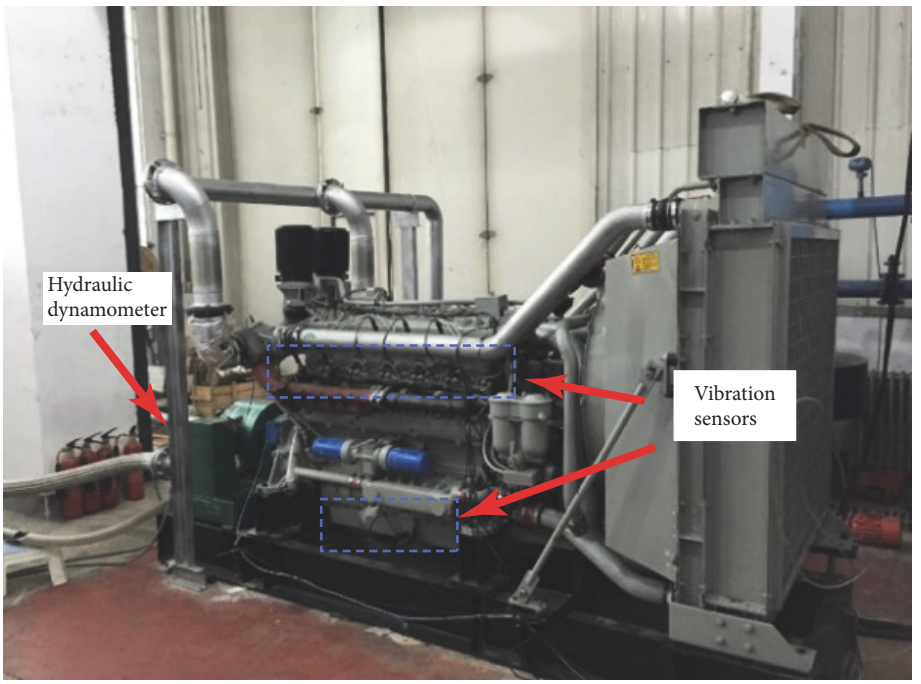

Figure 5: The 12-cylinder diesel engine for the fault simulation.

Table 3: Features of diesel engine.

Item	Value
Number of cylinders	12
Shape	V-shaped 60°
Firing sequence	B1-A1-B5-A5-B3-A3-B6-A6-B2-A2-B4-A4
Rating speed	2100 r/min
Rating power	485 kW
Rating exhaust volume	21.6 L
Cylinder diameter/stroke	128/140 mm

manually developed fault environment. A fault symptom signal could be reflected by the vibration and the transient rotation speed and could be captured by different sensors on the machine. The sensors, with a data acquisition frequency of 25600 Hz, were placed on the top of each cylinder head and on both sides of the crankshaft case. The vibration signals of the components in the running state were collected and transferred to the system and then were analyzed.

The diesel engine is one TBD234 twelve-cylinder V-shaped direct injection diesel engine, made in Henan Diesel Engine Industry Co. Ltd., Luoyang, China. The major features of the engine are summarized in Table 3.

In order to investigate the suggested approach, three different fault types were simulated that are cylinder knock fault, bearing wear fault, and cylinder score fault. For each fault simulation, the experiments were repeated eight times under the same environment but with different loads. The loads were supplied by a hydraulic dynamometer and were 0 N·m, 100 N·m, 200 N·m, 500 N·m, 600 N·m, 800 N·m, 1000 N·m, and 1200 N·m from group a to group h, respectively.

4.1.1. The Cylinder Knock Fault. In order to simulate the cylinder knock fault, the space between the piston and the cylinder head was filled with bronze ring. When the piston moved to the top dead point, the collision between the piston and the cylinder head would cause the impact damage to the engine, which could lead to the deformation of the piston and the crankshaft. Figure 6 illustrates the bronze ring before and after the impact with the piston.

In the simulation, the vibration speed and vibration acceleration signal values increased, and both the vibration speed and the vibration acceleration nodes were triggered and activated. The combination of the two different signals was used by system to diagnose the occurred fault. Comparisons between the fault and nonfault vibration speed values of each simulation group are illustrated in Figures 7(a)–7(h), while comparisons between the fault and nonfault vibration acceleration values of each group are illustrated in Figures 8(a)–8(h).

During the running of the engine, a combustion takes place in the combustion stroke and the resulted vibration is displayed every four strokes. In Figures 7 and 8, the waves in the areas indicated by numbers of each experiment group can be clearly observed, evaluating that vibration speed features and vibration acceleration features are able to diagnose cylinder knock fault, also proving that both features can be used for fault diagnosis. The cylinder knock fault diagnosis results of each experimental group based on the probabilistic graphical model can be seen in Table 4. It can be observed that cylinder knock fault was diagnosed with high accuracy.

Figure 6: Comparison of new bronze ring and ring after cylinder knock simulation.

4.1.2. The Bearing Wear Fault. Due to the contact and the impact between the conrod and the bent axle, force is exerted on the tile of the engine by the alternating load. In the experiment, in order to simulate the bearing wear fault, the tile was adjusted and the gap between the bearing and the tile was reduced, leading to a decrease in the transient rotation speed of the engine, an increase in kurtosis, and an increase in the vibration speed of the crankshaft case. The comparison of a new tile and a tile with wear surface after the experiment can be seen in Figure 9. Comparisons between the fault and nonfault vibration acceleration values of each simulation group are illustrated in Figures 10(a)–10(h), while the transient rotation speed can be seen in Figure 11. In order to have a succinct view of kurtosis trend, the relative value of the kurtosis was given and displayed in Figure 12. It came out after the calculation that was 0 minus the kurtosis value.

Table 4: Cylinder knock simulation diagnosis results.

Group Number	Cylinder Score	Cylinder Knock	Bearing Wear
a	0.253%	99.990%	0.263%
b	0.254%	99.990%	0.263%
c	0.039%	99.999%	0.263%
d	0.039%	99.989%	0.263%
e	0.259%	99.999%	0.263%
f	0.261%	99.992%	0.263%
g	0.039%	99.928%	0.263%
h	0.039%	98.540%	0.263%

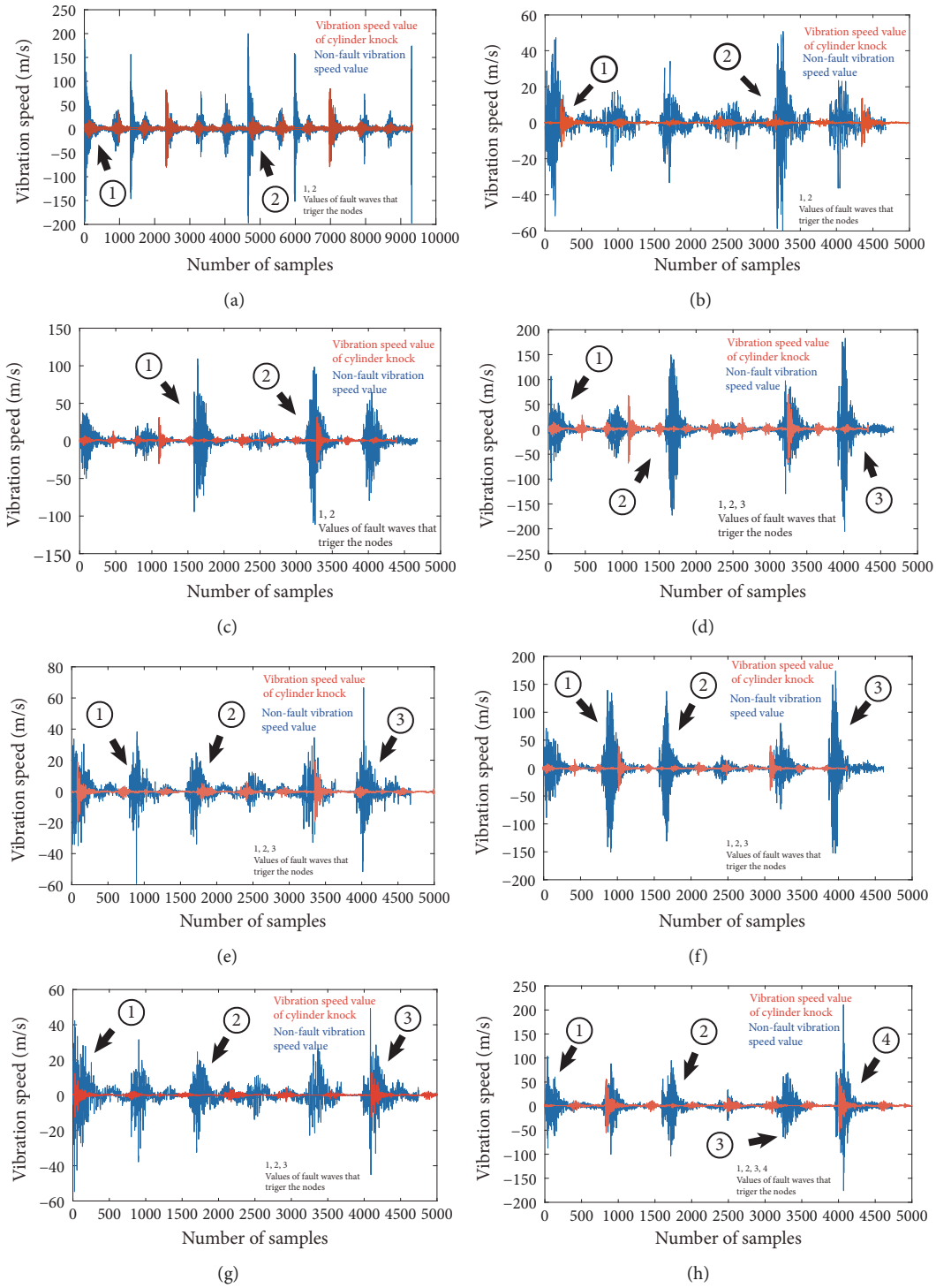

Figure 7: Comparison between fault and non-fault vibration speed values of cylinder knock fault ((a) with load of 0 N·m; (b) with load of 100 N·m; (c) with load of 200 N·m; (d) with load of 500 N·m; (e) with load of 600 N·m; (f) with load of 800 N·m; (g) with load of 1000 N·m; (h) with load of 1200 N·m).

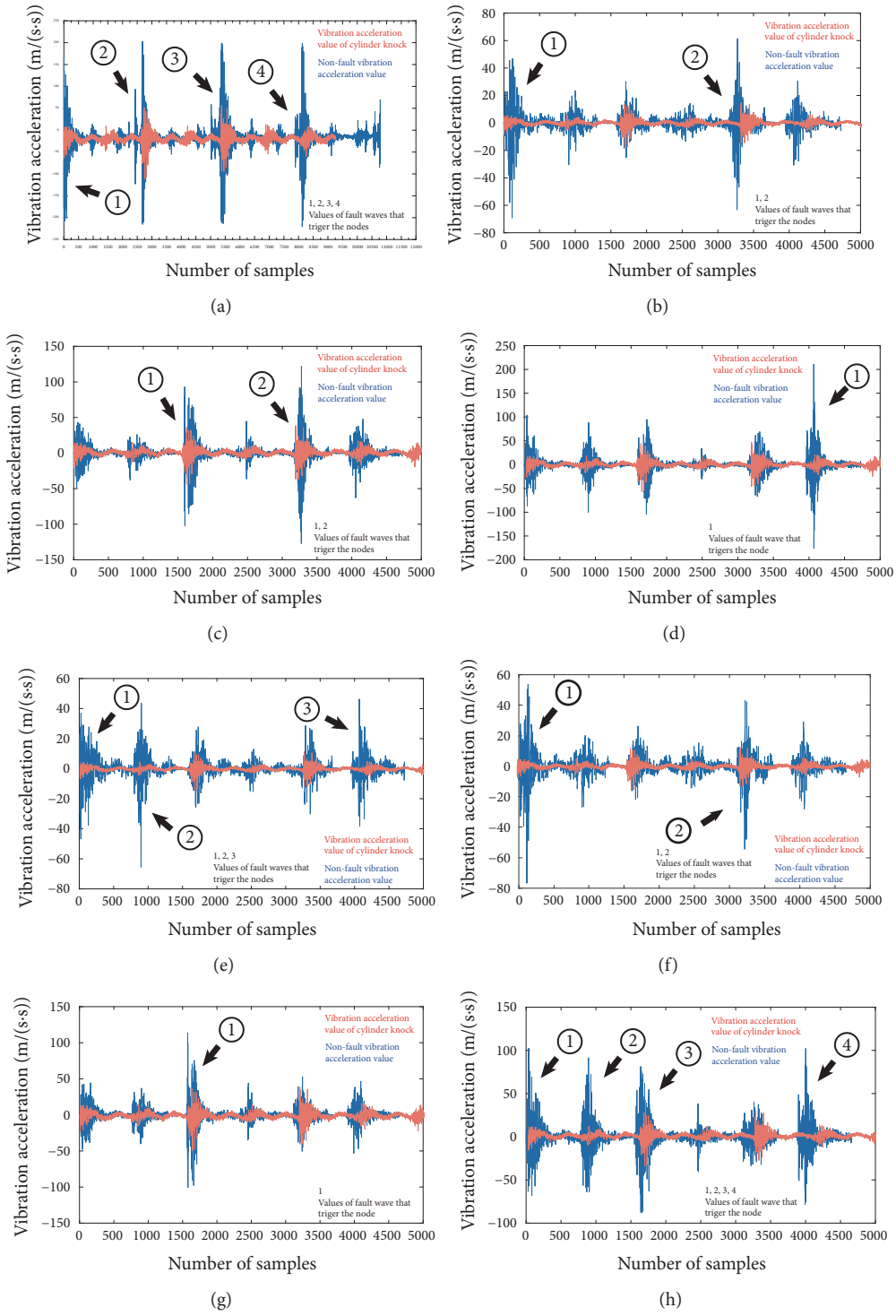

FIGURE 8: Comparison between fault and nonfault vibration acceleration values of cylinder knock fault ((a) with load of 0 N·m; (b) with load of 100 N·m; (c) with load of 200 N·m; (d) with load of 500 N·m; (e) with load of 600 N·m; (f) with load of 800 N·m; (g) with load of 1000 N·m; (h) with load of 1200 N·m).

The value of kurtosis was getting larger while the trend of the relative kurtosis went down as shown.

In Figures 10(a)–10(h), the waves of the fault simulation demonstrated high vibration speed values compared to the nonfault vibration waves, during all the four stroke running states, especially in the areas indicated by numbers. The initial setting of the transient rotation speed was at 1500 rpm, while, as it can be seen in Figure 11, the transient rotation speed during the fault simulation was lower than the setting due to the increase of the tile friction. In addition, the value of

Table 5: Bearing wear simulation diagnosis results.

Group Number	Cylinder Score	Cylinder Knock	Bearing Wear
a	0.328%	0.224%	99.998%
b	0.334%	0.224%	99.996%
c	0.039%	0.224%	99.989%
d	0.039%	0.224%	98.943%
e	2.806%	4.323%	97.460%
f	0.433%	1.037%	98.902%
g	3.607%	0.958%	87.448%
h	7.122%	0.224%	92.366%

Table 6: Cylinder score simulation diagnosis results.

Group Number	Cylinder score	Cylinder knock	Bearing wear
a	99.979%	0.854%	2.422%
b	99.992%	0.224%	2.423%
c	99.973%	0.870%	2.427%
d	99.960%	0.224%	2.436%
e	97.626%	0.854%	0.263%
f	98.898%	0.224%	0.263%
g	96.782%	0.875%	0.263%
h	94.344%	0.224%	0.263%

Figure 9: Comparison of a new tile and a tile after the wear simulation.

kurtosis increased for all groups while the relative value of kurtosis decreased. The bearing wear diagnosis results for each experimental group can be seen in Table 5. The features of bearing wear fault, which are reflected by the changes of vibration speed, transient rotation speed, and kurtosis, were clearly proved to be able to diagnose the bearing wear fault. It can be used for the diagnosis, and the diagnosis based on the probabilistic graphical model was achieved with high accuracy.

4.1.3. The Cylinder Score Fault. In the cylinder score fault case, the friction between the piston and the cylinder was increased for the test simulation. This led to an increase in the vibration acceleration values and an increase in the torsional vibration. In Figure 13, the piston surface after the score fault simulation is illustrated. The vibration acceleration signals of the fault for each group can be seen in Figures 14(a)–14(h), while the torsional vibration values are illustrated in Figure 15.

In 8 groups of Figure 14, the waves of vibration acceleration appeared in the areas indicated by numbers. In Figure 15, the peak values of torsional vibration amplitude of all groups were found higher compared to the values of the nonfault running state. The features of cylinder score fault were proved to be able to diagnose the fault, and the diagnosis based on the probabilistic graphical model was achieved with high accuracy. The cylinder score diagnosis results for each experimental group can be seen in Table 6.

5. Discussion

The average percentages of each fault category in the simulation environment can be seen in Table 7. The results demonstrated that the diagnosis correction rates of cylinder knock fault, bearing wear, and cylinder score were 99.80%, 96.89%, and 98.44%, respectively. Basically, a type of fault can be determined based on the rule that the largest fault probability is larger than a certain threshold ε. The initial value of ε can be determined by experts, and it is suggested

Table 7: The average result for each kind of fault.

Diagnosis result	Cylinder score	Cylinder knock	Bearing wear
Cylinder knock fault simulation	0.15%	99.80%	0.26%
Bearing wear simulation	3.09%	0.93%	96.89%
Cylinder score simulation	98.44%	0.54%	1.35%

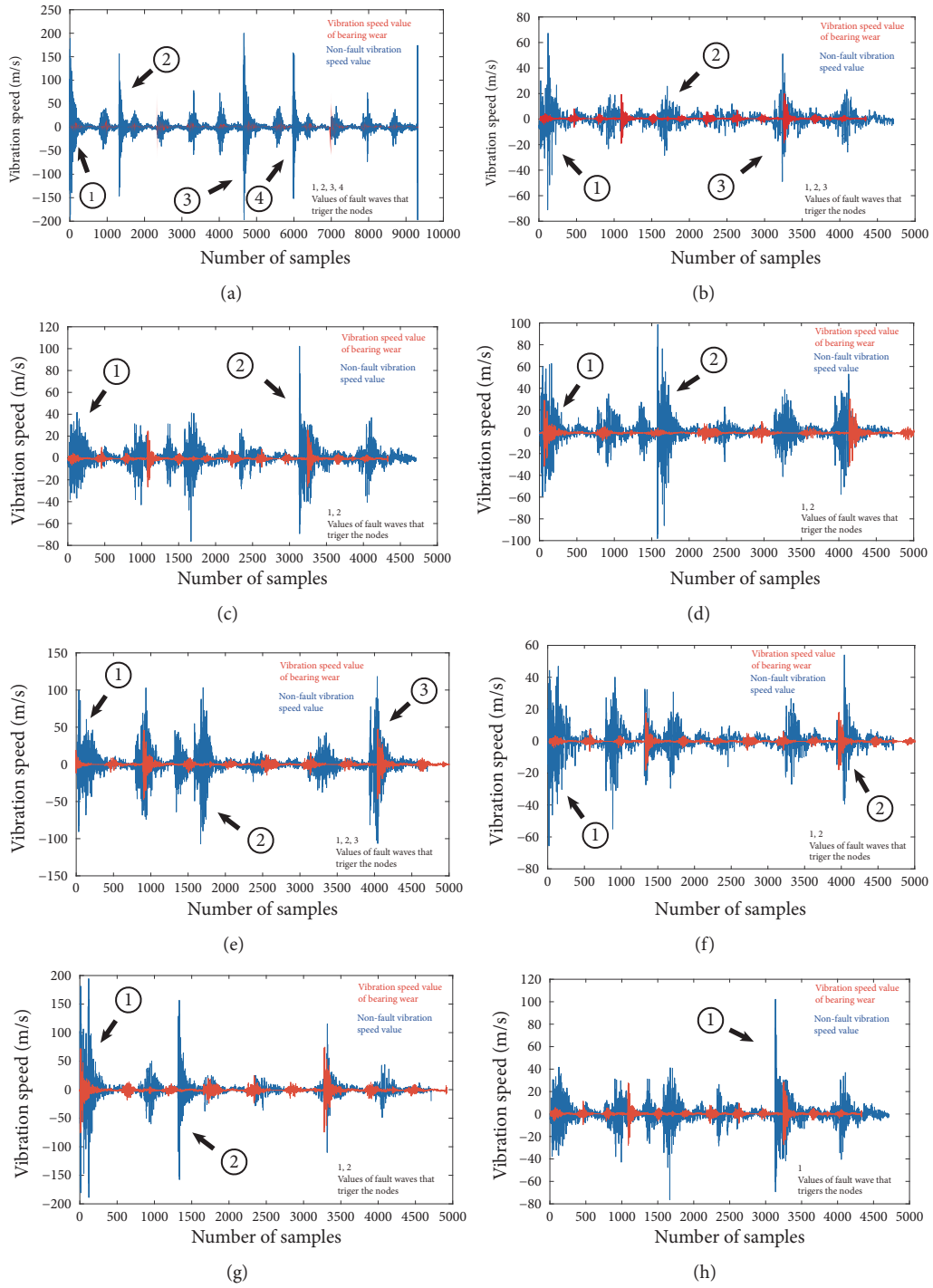

Figure 10: Comparison between fault and nonfault vibration speed values of bearing wear fault ((a) with load of 0 N·m; (b) with load of 100 N·m; (c) with load of 200 N·m; (d) with load of 500 N·m; (e) with load of 600 N·m; (f) with load of 800 N·m; (g) with load of 1000 N·m; (h) with load of 1200 N·m).

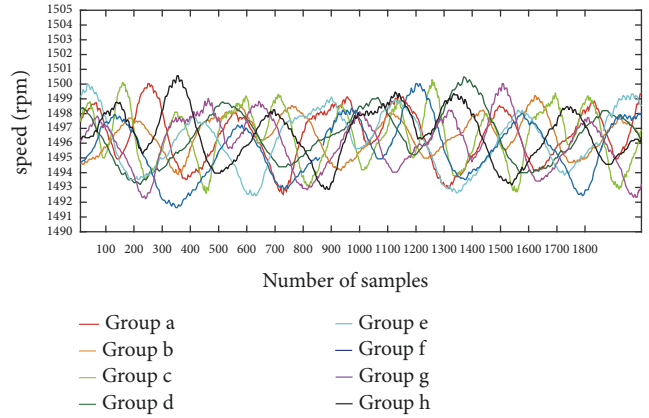

Figure 11: Transient rotation speed of bearing wear fault for each group.

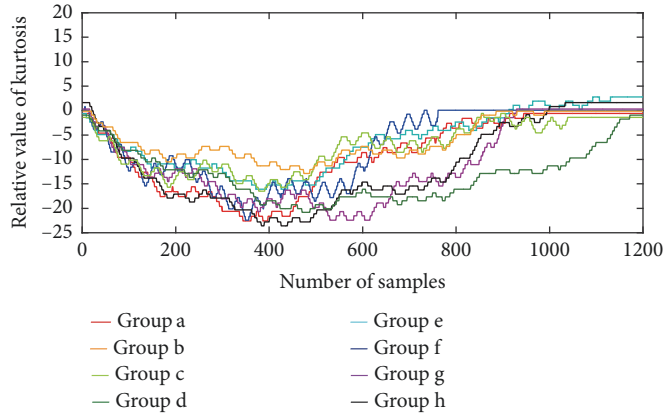

Figure 12: Relative kurtosis values (0 minus kurtosis) of bearing wear fault for each group.

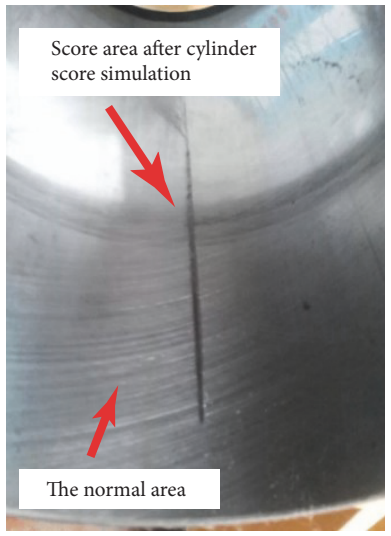

Figure 13: Comparison between a normal area and an area damaged from the cylinder score simulation.

to be 80% at the beginning for the ICE fault diagnosis. All the faults were distinguished successfully with high accuracy.

The diagnosis results were compared to the results that are processed and calculated with incomplete information. Single symptom can not distinguish fault type since the fault of cylinder knock and the fault of cylinder score have the same symptom that is vibration acceleration, while the fault of cylinder knock and the fault of bearing wear have the same symptom that is vibration speed. For the fault of cylinder knock, the vibration speed and vibration acceleration are also characters for other two faults. The probabilities of it were 88% and 76%, respectively, when two symptoms appeared separately. For the fault of cylinder score, it could not be distinguished only with the symptom of vibration acceleration. The probability of cylinder score was 89% when the character of vibration acceleration appeared alone and was 79% when the symptom of torsional vibration appeared alone. For the fault of bearing wear, although the transient rotation speed and kurtosis can be used for diagnosis when they appeared as fault symptom separately, the probability was only 67% and 85%, respectively. The probability was 85% when only the vibration speed symptom appeared. All the percentages of each type of fault are lower than proposed results. The suggested fault diagnosis method with the work of nodes together demonstrated good performance and high accuracy.

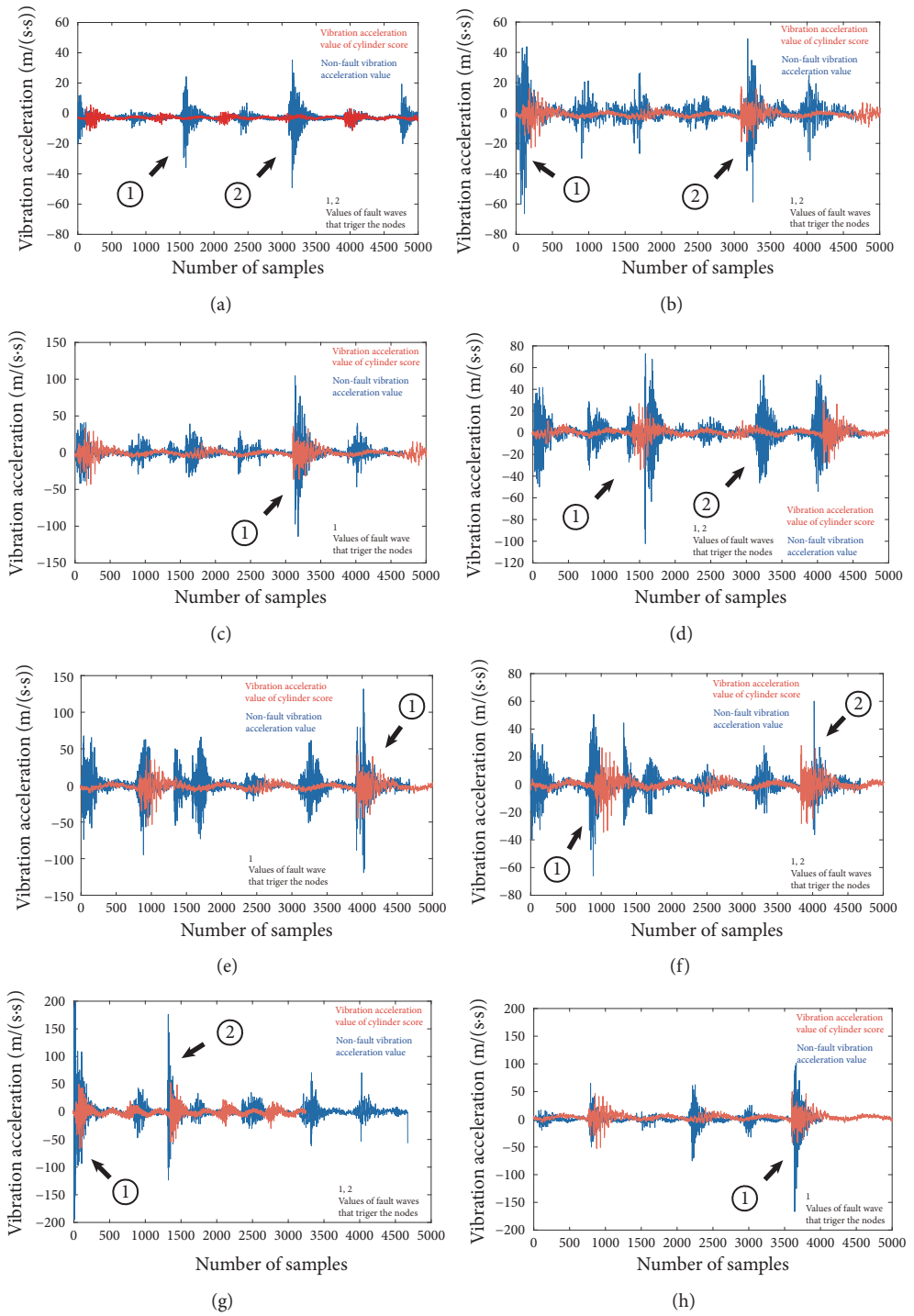

FIGURE 14: Comparison between fault and non-fault vibration acceleration values of cylinder score fault ((a) with load of 0 N·m; (b) with load of 100 N·m; (c) with load of 200 N·m; (d) with load of 500 N·m; (e) with load of 600 N·m; (f) with load of 800 N·m; (g) with load of 1000 N·m; (h) with load of 1200 N·m).

In further work, the fault categories can be expanded in the model, and the diagnosis network can be built with more diagnosis evidences. The capacity of the ICE fault diagnosis model can be improved.

6. Conclusion

A method for ICE fault diagnosis using the probabilistic graphical model was presented. Three types of machine faults and five symptoms were connected based on a three-layer

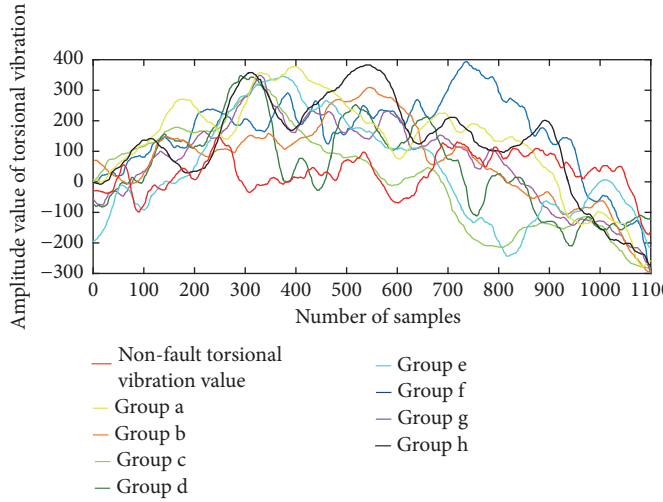

Figure 15: Torsional vibration amplitude values of cylinder score fault.

network. The combination of various engine signals was used for diagnosing faults that may occur, and the use of leak probability with Noisy-OR gate improved the diagnosis accuracy. A 12-cylinder diesel engine was manually adjusted to simulate real fault cases of cylinder knock, bearing wear, and cylinder score. The output of the diagnosis method showed high diagnosis accuracy in the results presented in percentages.

Data Availability

The data used to support the findings of this study are included within the article.

Conflicts of Interest

The authors declare that there are no conflicts of interest regarding the publication of this paper.

Acknowledgments

This research has been supported by the National Research Program of China (863 Program) (no. 2014AA041806) and the National Key Research and Development Plan (no. 2016YFF0203305).

References

[1] S. Liu, R. Du, and S. Yang, "Fault diagnosis for diesel engines by wavelet packets analysis of vibration signal measured on cylinder head," *Journal of Vibration Engineering*, vol. 04, pp. 85–92, 2000.

[2] J.-D. Wu and J.-C. Chen, "Continuous wavelet transform technique for fault signal diagnosis of internal combustion engines," *NDT & E International*, vol. 39, no. 4, pp. 304–311, 2006.

[3] L. Bo, H. Pan, and X. Li, "An expert system for fault diagnosis in diesel engine based on wavelet packet analysis and hybrid PSO-DV based neural network," in *Proceedings of the 2010 International Conference on Intelligent Computing and Cognitive Informatics, ICICCI 2010*, pp. 29–32, Malaysia, June 2010.

[4] L. Song, H. Wang, and P. Chen, "Vibration-based intelligent fault diagnosis for roller bearings in low-speed rotating machinery," *IEEE Transactions on Instrumentation and Measurement*, vol. 67, no. 8, pp. 1887–1899, 2018.

[5] X. Wang, C. Liu, F. Bi, X. Bi, and K. Shao, "Fault diagnosis of diesel engine based on adaptive wavelet packets and EEMD-fractal dimension," *Mechanical Systems and Signal Processing*, vol. 41, no. 1-2, pp. 581–597, 2013.

[6] J.-D. Wu and C.-H. Liu, "An expert system for fault diagnosis in internal combustion engines using wavelet packet transform and neural network," *Expert Systems with Applications*, vol. 36, no. 3, pp. 4278–4286, 2009.

[7] Z. K. Peng and F. L. Chu, "Application of the wavelet transform in machine condition monitoring and fault diagnostics: a review with bibliography," *Mechanical Systems and Signal Processing*, vol. 18, no. 2, pp. 199–221, 2004.

[8] Y. Hao, L. Song, L. Cui, and H. Wang, "A three-dimensional geometric features-based SCA algorithm for compound faults diagnosis," *Measurement*, vol. 134, pp. 480–491, 2019.

[9] L. Cui, J. Wang, and S. Lee, "Matching pursuit of an adaptive impulse dictionary for bearing fault diagnosis," *Journal of Sound and Vibration*, vol. 333, no. 10, pp. 2840–2862, 2014.

[10] L. Cui, X. Wang, H. Wang, and N. Wu, "Improved fault size estimation method for rolling element bearings based on concatenation dictionary," *IEEE Access*, vol. 7, pp. 22710–22718, 2019.

[11] L. Cui, J. Huang, F. Zhang, and F. Chu, "HVSRMS localization formula and localization law: Localization diagnosis of a ball bearing outer ring fault," *Mechanical Systems and Signal Processing*, vol. 120, pp. 608–629, 2019.

[12] H. Wang, S. Li, L. Song, and L. Cui, "A novel convolutional neural network based fault recognition method via image fusion of multi-vibration-signals," *Computers in Industry*, vol. 105, pp. 182–190, 2019.

[13] X. Wang, H. Yu, S. Duan, and J. Yan, "Study on diesel engine fault diagnosis based on integration of Bayesian and genetic neural network method," *Advanced Materials Research*, vol. 311-313, pp. 2277–2281, 2011.

[14] Z. Tong, X. Zhang, A. Dong, X. Shi, and J. Du, "Improved clustering algorithms used in diesel engine vibration fault diagnosis based on bayesian networks," *Lecture Notes in Electrical Engineering*, vol. 238, pp. 2111–2118, 2014.

[15] T. Bodisco, R. Reeves, R. Situ, and R. Brown, "Bayesian models for the determination of resonant frequencies in a di diesel engine," *Mechanical Systems and Signal Processing*, vol. 26, no. 1, pp. 305–314, 2012.

[16] L. Song, H. Wang, and P. Chen, "Step-by-step Fuzzy diagnosis method for equipment based on symptom extraction and trivalent logic fuzzy diagnosis theory," *IEEE Transactions on Fuzzy Systems*, vol. 26, no. 6, pp. 3467–3478, 2018.

[17] A. Widodo and B. Yang, "Support vector machine in machine condition monitoring and fault diagnosis," *Mechanical Systems and Signal Processing*, vol. 21, no. 6, pp. 2560–2574, 2007.

[18] C. Cai, C. Zhang, and L. Gang, "A novel fault diagnosis approach combining SVM with association rule mining for ship diesel engine," in *Proceedings of the 2016 IEEE International Conference on Information and Automation, IEEE ICIA 2016*, pp. 130–135, China, August 2016.

[19] L. Cui, X. Wang, Y. Xu, H. Jiang, and J. Zhou, "A novel Switching Unscented Kalman Filter method for remaining useful life prediction of rolling bearing," *Measurement*, vol. 135, pp. 678–684, 2019.

[20] J. Kowalski, B. Krawczyk, and M. Woźniak, "Fault diagnosis of marine 4-stroke diesel engines using a one-vs-one extreme learning ensemble," *Engineering Applications of Artificial Intelligence*, vol. 57, pp. 134–141, 2017.

[21] H. Wang, P. Wang, L. Song, B. Ren, and L. Cui, "A novel feature enhancement method based on improved constraint model of online dictionary learning," *IEEE Access*, vol. 7, pp. 17599–17607, 2019.

[22] Y.-S. Yang, A.-B. Ming, Y.-Y. Zhang, and Y.-S. Zhu, "Discriminative non-negative matrix factorization (DNMF) and its application to the fault diagnosis of diesel engine," *Mechanical Systems and Signal Processing*, vol. 95, pp. 158–171, 2017.

[23] H. L. Gelgele and K. Wang, "An expert system for engine fault diagnosis: Development and application," *Journal of Intelligent Manufacturing*, vol. 9, no. 6, pp. 539–545, 1998.

[24] V. Macián, B. Tormos, A. Sala, and J. Ramirez, "Fuzzy logic-based expert system for diesel engine oil analysis diagnosis," *Insight: Non-Destructive Testing and Condition Monitoring*, vol. 48, no. 8, pp. 462–469, 2006.

[25] P. Nabende and T. Wanyama, "An expert system for diagnosing heavy-duty diesel engine faults," in *Proceedings of the 2007 International Conference on Systems, Computing Sciences and Software Engineering, SCSS 2007, Part of the International Joint Conferences on Computer, Information, and Systems Sciences, and Engineering, CISSE 2007*, pp. 384–389, USA, December 2007.

[26] A. Abdollahi, K. R. Pattipati, A. Kodali, S. Singh, S. Zhang, and P. B. Luh, "Probabilistic graphical models for fault diagnosis in complex systems," in *Principles of Performance and Reliability Modeling and Evaluation*, Springer Series in Reliability Engineering, pp. 109–139, Springer International Publishing, 2016.

[27] A. Oniśko, M. J. Druzdzel, and H. Wasyluk, "Learning Bayesian network parameters from small data sets: Application of Noisy-OR gates," *International Journal of Approximate Reasoning*, vol. 27, no. 2, pp. 165–182, 2001.

[28] M. Pradhan, G. Provan, B. Middleton, and M. Henrion, "Knowledge engineering for large belief networks," in *Proceedings of the Tenth International Conference on Uncertainty in Artificial Intelligence*, pp. 484–490, 1994.

[29] A. Zagorecki and M. J. Druzdzel, "Knowledge engineering for bayesian networks: how common are noisy-max distributions in practice," *IEEE Transactions on Systems, Man, and Cybernetics: Systems*, vol. 43, no. 1, pp. 186–195, 2013.

[30] D. S. Paolino, A. Tridello, G. Chiandussi, and M. Rossetto, "Estimation of P-S-N curves in very-high-cycle fatigue: Statistical procedure based on a general crack growth rate model," *Fatigue & Fracture of Engineering Materials & Structures*, vol. 41, no. 4, pp. 718–726, 2018.

[31] H. Feng, Y. Wang, and X. Jiang, "A Maximum Likelihood method for estimating probabilistic strain amplitude–fatigue life curves," *Acta Mechanica Solida Sinica*, vol. 31, no. 1, pp. 80–93, 2018.

[32] OREDA, "Offshore and onshore reliability data handbook," in *Topside Equipment*, vol. 1, pp. 167–184, DNV GL, OREDA Participants, 6th edition, 2015.

[33] Y. Zhao, F. Xiao, and S. Wang, "An intelligent chiller fault detection and diagnosis methodology using Bayesian belief network," *Energy and Buildings*, vol. 57, pp. 278–288, 2013.

[34] D. T. Hountalas, "Prediction of marine diesel engine performance under fault conditions," *Applied Thermal Engineering*, vol. 20, no. 18, pp. 1753–1783, 2000.

[35] R. Antonić, Z. Vukić, and O. Kuljača, "Marine diesel engine faults diagnosis based on observed symptoms and expert knowledge," in *Proceedings of the 6th IFAC Conference on Manoeuvring and Control of Marine Craft : MCMC'03*, vol. 36, pp. 133–138, 2003.

[36] B. Ma and B. B. Zhai, "Dynamic response analysis on connecting rod bearing shell of reciprocating machinery with abrasion fault," *Mechanical Science Technology for Aerospace Engineering*, vol. 36, no. 12, pp. 1843–1851, 2017.